Low-energy electron scattering by methylsilane

M. H. F. Bettega
Departamento de Física, Universidade Federal do Paraná, Caixa Postal 19044, 81531-990, Curitiba, Paraná, Brazil

C. Winstead[a] and V. McKoy
A. A. Noyes Laboratory of Chemical Physics, California Institute of Technology, Pasadena, California 91125

(Received 28 January 2003; accepted 31 March 2003)

We report calculated elastic and inelastic cross sections for low-energy electron collisions with methylsilane, CH_3SiH_3, obtained using the Schwinger multichannel method. The elastic cross sections, obtained within the static-exchange approximation, are compared with elastic results for C_2H_6 and Si_2H_6. Electron-impact excitation cross sections were computed for sixteen electronic states arising from excitation out of the two highest-lying valence orbitals. The dissociation of the lowest few states was examined through limited electronic-structure calculations, which indicated that the $2\,^{1,3}A_1$ states dissociate to CH_3SiH+H_2 while the $1\,^{1,3}E$ states dissociate to CH_3+SiH_3.
 [DOI: 10.1063/1.1576382]

I. INTRODUCTION

Methylsilane (CH_3SiH_3) is widely used as a precursor gas in plasma-enhanced chemical vapor deposition (PECVD),[1] primarily for the synthesis of plasma-polymerized methylsilane films[2] for use as photoresists or, at higher substrate temperatures, of silicon carbide layers.[3] More recently, CH_3SiH_3 has also been studied as a precursor for PECVD of organosilicate layers useful as low-k dielectrics.[4] In modeling a discharge environment, one needs as input information on all basic processes that occur in the plasma, including the cross sections for elastic and inelastic electron–molecule collisions.[5] The electronic-excitation cross sections are important because excitation to dissociative electronic states promotes the generation of reactive neutral fragments, while the cross section for electronically elastic scattering largely determines electron transport properties. However, despite its technological importance, very little is yet known about electron collisions with CH_3SiH_3. Computational studies have mainly been devoted to the calculation of ground-state electronic structure and properties[6] or to reactions.[7] Indeed, we are aware of only one previous calculation[8] that addressed electronic excitation of CH_3SiH_3. Experimental studies have likewise concentrated on the properties and vibrational spectroscopy of the ground electronic state. However, a few studies have been done of the ultraviolet photoabsorption spectrum[9–11] and photodissociation chemistry.[13–15] To our knowledge, no electron cross sections, experimental or theoretical, are yet available for CH_3SiH_3 (a preliminary account of our elastic results appears elsewhere[12]).

We report here results from a study of elastic and inelastic collisions of low-energy electron with methylsilane. In this work, we employed the Schwinger multichannel method[16,17] as implemented for parallel computers.[18,19] The elastic integral, differential, and momentum-transfer cross sections were obtained in the static-exchange approximation for energies up to 50 eV. The static-exchange approximation generally works well for energies in this energy range except at energies below ~5 eV or in the presence of shape resonances, which it shifts to higher energies (typically by 1–4 eV) and broadens. Inelastic cross sections were obtained within a few-channel approximation for a variety of low-lying singlet and triplet excited states at energies from threshold up to 50 eV. We also carried out limited electronic structure calculations in order to investigate the dissociation of some of the excited electronic states.

II. COMPUTATIONAL DETAILS

The SMC method and its implementation for parallel computers have been discussed in several publications.[16–19] Here we give details specific to the present calculations.

In all of our calculations except studies of excited-state dissociation, the nuclei were fixed at the ground-state equilibrium geometry, which belongs to the C_{3v} point group. For most calculations we used the geometry as optimized using second-order Møller–Plesset perturbation theory, the 6-31+G(d) basis set, and GAMESS,[20] while for a few ($7a1 \rightarrow 4e$ calculations) we used the experimental geometry;[21] the slight differences between these two geometries will have no significant effect on our results.

To obtain information about the excited electronic states of CH_3SiH_3, we carried out single-excitation configuration-interaction (SECI) calculations using GAUSSIAN 98[22] and its built-in 6-311++G($3d$,$2p$) basis set. This extended basis set should be flexible enough to give nearly converged results for the lowest few states of each spin and symmetry, whereas the otherwise similar calculations of Gordon,[8] carried out with various smaller basis sets, showed considerable basis-set dependence. In fact, we find overall qualitative agreement with Gordon's results for the energies and character of the lowest excited states, though with a few significant differences; in particular, we predict markedly lower thresholds for the $1,2\,^3E$ and $1\,^{1,3}A_2$ states. We find, as did Gordon, that the lowest excited states involve excitation not only out of the

[a]Electronic mail: carl@schwinger.caltech.edu

TABLE I. Properties of some low-lying excited states of CH_3SiH_3.

State	Principal character	Vertical threshold (eV)			Oscillator strength	
		SECI	IVO	Expt.[a]	SECI	IVO
$2\,^3A_1$	$7a_1\rightarrow 8a_1$	8.52	8.95[b]			
$1\,^3E$	$3e\rightarrow 8a_1$	8.59	9.28			
$2\,^3E$	$3e\rightarrow 9a_1$	8.94	9.80			
$1\,^3A_2$	$3e\rightarrow 4e$	8.97	9.32[b]			
$3\,^3A_1$	$7a_1\rightarrow 9a_1$, $3e\rightarrow 4e$	9.09	10.14[b]			
$2\,^1A_1$	$7a_1\rightarrow 8a_1$	9.16	9.25	7.87	0.149	0.115
$1\,^1E$	$3e\rightarrow 8a_1$	9.47	9.90[b]	8.78	0.144	0.323[b]
$2\,^1E$	$3e\rightarrow 9a_1$	9.75	10.14[b]	9.15	0.295	0.146[b]
$1\,^1A_2$	$3e\rightarrow 4e$	9.81	9.92		0.0	0.0
$3\,^3E$	$7a_1\rightarrow 4e$, $3e\rightarrow 4e$	9.33	10.16			
$3\,^1E$	$7a_1\rightarrow 4e$	10.11	10.32[b]		0.066	0.058[c]
$3\,^1A_1$	$7a_1\rightarrow 9a_1$	10.14	10.40		0.409	0.305

[a]Reference 11.
[b]Computed with the orbital optimized for the other spin state having the same configuration.
[c]Computed with triplet IVO at MP2/6-31+G(d) geometry and including all 6 d-type orbitals.

highest occupied molecular orbital, the $7a_1$ Si–C bonding orbital, but also out of the next-highest orbital, $3e$, which is Si–H bonding. In most of the low-lying excited states, either $(7a_1)^{-1}$ or $(3e)^{-1}$ character predominates, but a few, including $3\,^{1,3}A_1$ and $3\,^3E$, are significantly mixed. That excitation both from $7a_1$ and from $3e$ is important reflects the nearly equal binding energies of these orbitals: Their respective Koopmans ionization potentials are 12.4 and 12.7 eV, as determined from the restricted Hartree–Fock (RHF) calculation described immediately below, while photoelectron spectroscopy[11] gives vertical ionization potentials of 11.6 and 12.1 eV, respectively. Information on the lowest excited states is listed in Table I; except as noted for $3\,^1E$, improved virtual orbital (IVO) results are computed using the same wavefunctions as in the scattering calculations.

The molecular ground state was described by a single-configuration RHF wave function. The basis set used was, in the standard notation, the 6-311++G($3d$,$2p$) basis set as defined in the program GAMESS[20] (which differs slightly from the basis set of the same name in Gaussian[22]). In most calculations, all six Cartesian components of the d functions were included, giving a total of 182 primitive and 138 contracted Cartesian Gaussian functions for CH_3SiH_3. In the $7a_1\rightarrow 4e$ calculations, the $3s$-type combination of d functions was excluded, reducing the size of the basis set by 6 functions.

We obtained 0.727 D as the RHF value of the permanent electric dipole moment, which compares well with the experimental value of 0.735 D.[21] A dipolar field causes elastic scattering in long-range collisions, an effect not fully captured in our SMC calculation, which employs square-integrable trial functions. We accordingly incorporated a correction for such long-range scattering using well-known techniques based on the dipole-Born approximation.[23] To suppress the divergence of the elastic dipole-Born amplitude in the forward direction, we included a small, arbitrary inelasticity. Neither the integral cross section nor the differential cross section away from the extreme forward direction was sensitive to the precise value of this energy loss, which was set at 0.001 hartree in the results reported below. We retained partial waves up to $\ell=5$, $m=5$ from the SMC calculation in computing the dipole-corrected results; below 10 eV, neither the differential nor the integral cross sections were sensitive to the exact value of this partial-wave cutoff except at the very lowest energies. Above 10 eV, the range of forward angles over which the dipole correction is non-negligible is increasingly small, while, on the other hand, higher partial waves from the SMC calculation are increasingly necessary to describe the near-backward scattering. We, therefore, omitted the dipole-Born correction to the elastic cross section above 10 eV.

Elastic scattering was described in the static-exchange approximation; that is, we neglected polarization of the target molecule by the projectile electron but solved the full many-electron scattering problem defined by the charge density of the RHF ground state. For comparison purposes, we also computed elastic electron cross sections for disilane, Si_2H_6, and ethane, C_2H_6, under the same conditions as for CH_3SiH_3, i.e., using the static-exchange approximation, the 6-311++G($3d$,$2p$) basis set, and the respective ground-state equilibrium geometries.[24,25]

To describe the excited states of CH_3SiH_3, we used the improved virtual orbital (IVO) approximation.[26] In the collision calculations, a common IVO was used to describe singlet and triplet excited states having the same nominal configuration; excitation thresholds were computed using that common orbital and the appropriate (singlet or triplet) Hamiltonian. For the $(7a_1\rightarrow 8a_1)\,^{1,3}A_1$ and $(7a_1\rightarrow 9a_1)\,^{1,3}A_1$ states, the singlet IVO was used, while for the $(3e\rightarrow 8a_1)\,^{1,3}E$, $(3e\rightarrow 9a_1)\,^{1,3}E$, and $(7a_1\rightarrow 4e)\,^{1,3}E$ states, the triplet IVO was used. The $3e\rightarrow 4e$ excitation produces six states: $^{1,3}A_1$, $^{1,3}E$, and $^{1,3}A_2$. For that case, we carried out a singlet IVO calculation for the $^1A_2$ state and used the resulting $4e$ orbital pair to form all eight possible hole-particle and spin combinations. Each such combination

was treated as a scattering channel, with the $^1A_2$ IVO energy as a common threshold for the four singlets and the $^3A''$ energy computed using that IVO as a common threshold for the four triplets. (Although limitations of GAMESS resulted in the $3e \rightarrow 4e$ triplet energy calculation incorporating unwanted "extra" configurations, the natural-orbital occupancies showed that the effect was very slight.) Proper $(3e \rightarrow 4e)$ $^{1,3}A_1$, $^{1,3}E$, and $^{1,3}A_2$ states were formed at the end of the calculation by taking appropriate linear combinations of the channels.

The excitation thresholds obtained from the IVO calculations just described are shown in Table I together with the SECI and experimental values. Where comparison is possible, the SECI results are significantly above the experimental values. Because the IVO approximation is a restricted form of SECI, it must give poorer results, but generally the additional error is moderate.

Excitation cross sections were computed in six separate few-channel calculations, in each of which the elastic channel was coupled to the singlet and triplet channels associated with a given one-particle excitation. Taking into account the degeneracy of the E representation, the inelastic scattering calculations thus coupled either three channels (for $7a_1 \rightarrow na_1$ excitations), five channels (for $3e \rightarrow na_1$ and $7a_1 \rightarrow 4e$ excitations), or nine channels $(3e \rightarrow 4e)$.

Optically-allowed transitions may be excited in long-range collisions between the electron and the target, an effect that may be taken into account by applying a dipole-Born[23] correction analogous to that used for the elastic channel, but based on the transition dipole rather than on the ground-state permanent dipole. We applied such corrections to electron-impact excitation of the $(7a_1 \rightarrow 8a_1)$ $^1A_1$, $(7a_1 \rightarrow 9a_1)$ $^1A_1$, $(3e \rightarrow 8a_1)$ ^1E, and $(3e \rightarrow 9a_1)$ ^1E states, using the IVO length-form transition dipoles corresponding to the oscillator strengths listed in Table I and retaining partial waves up to $\ell = 5$, $m = 4$ from the SMC calculation. The remaining states considered here are either optically forbidden or have small oscillator strengths in the SECI approximation (except in the special case of $3e \rightarrow 4e$ discussed immediately below).

The $(3e \rightarrow 4e)$ 9-channel calculation produced an unusually large ^1E cross section, with a peak value of about 1.7×10^{-16} cm^2 and a slow fall-off at higher energies, even before applying a dipole-scattering correction. This behavior correlated with a very large oscillator strength, 1.01, computed using the same description of the ^1E state. On closer examination, we found that using the ^1E potential instead of the $^1A_2$ produces a very different $4e$ IVO and a much smaller oscillator strength. Moreover, the SECI calculations indicate no $^{1,3}E$ or $^{1,3}A_1$ states having a clear $3e \rightarrow 4e$ one-particle character. The $(3e \rightarrow 4e)$ $^{1,3}E$ and $^{1,3}A_1$ cross sections obtained from our 9-channel calculation, therefore, cannot be considered physical. On the other hand, the $1\,^3A_2$ state is well described as a $3e \rightarrow 4e$ single-particle excitation, and an IVO-type calculation for that state produces a $4e$ orbital highly similar to that obtained for $^1A_2$. We thus report below only the $^{1,3}A_2$ cross sections from the $(3e \rightarrow 4e)$ calculation.

Although detailed investigation of dissociation following excitation of CH_3SiH_3 is outside the scope of the present electron-collision study, we did carry out limited calculations on selected excited states using GAMESS, its internal 6-31+G(d) basis set, and complete-active-space self-consistent field (CASSCF) wave functions with six active electrons in seven active orbitals. The calculations were run as geometry optimizations beginning at the vertical (ground state) geometry, with the wave function restricted to one of the two representations (A' or A'') of the C_s point group. At the initial geometry, the active orbitals thus comprised the $3e$ and $7a_1$ occupied orbitals together with $8a_1$, $4e$, and $9a_1$ virtual orbitals. Such limited calculations cannot identify every important dissociation channel, nor can they identify secondary dissociations and rearrangements, but they can identify barrier-free dissociation pathways on repulsive surfaces and so provide some useful insights.

The CASSCF optimization in $^3A'$ showed that the lowest excited state, $(7a_1 \rightarrow 8a_1)$ $2\,^3A_1$, can dissociate without a barrier to methyl and silyl radicals. A calculation for the $2\,^1A_1$ state proceeded to a geometry with the Si–C bond stretched to 2.74 Å before encountering convergence difficulties, suggesting that that state also dissociates to $CH_3 + SiH_3$. On the other hand, calculations in $^1A''$ and $^3A''$ for one component of each of the $(3e \rightarrow 8a_1)$ $1\,^{1,3}E$ states both proceeded downhill to H_2 and singlet or triplet CH_3SiH radicals. These results are consistent with the Si–C bonding character of the $7a_1$ orbital and Si–H bonding character of the $3e$ orbital. Computational study of higher-lying states within the $^{1,3}A_1$ and $^{1,3}E$ manifolds is more difficult and was not carried out; however, we anticipate that some fraction of excitation to such higher-lying states will result in dissociation on the $2\,^{1,3}A_1$ and $1\,^{1,3}E$ surfaces due to conical intersections and/or radiative transitions.

We may compare our dissociation results to the photochemical studies of Longeway and Lampe[15] using 147 nm (8.43 eV) photons. Reference to the photoabsorption spectrum[11] indicates that 8.43 eV is well above the peak absorption of the first singlet excited state, $(7a_1 \rightarrow 8a_1)$ $2\,^1A_1$, and well into the low-energy shoulder of the second singlet state, $(3e \rightarrow na_1)$ $1\,^1E$, which we found to dissociate into $CH_3SiH + H_2$. Consistent with our calculations, Longeway and Lampe deduced that 69% of the primary photodissociation preserved the Si–C bond, with the products being, in order of decreasing quantum yield, $CH_2SiH_2 + H_2$, $CH_3SiH + H_2$, $CHSiH_3 + H_2$, and $CH_3SiH + 2H$, while the remaining 31% of primary dissociation produced $CH_3 + H + SiH_2$ and to a lesser extent $CH_4 + SiH_2$.

III. RESULTS AND DISCUSSION

A. Elastic scattering

Figure 1 shows the elastic integral cross section (ICS) for CH_3SiH_3, along with its decomposition into C_{3v} symmetry components. Although Fig. 1 shows only the summed cross section for ^2E, it may be noted that its two components, which are not equivalent from the point of view of the numerical quadratures used, were computed independently

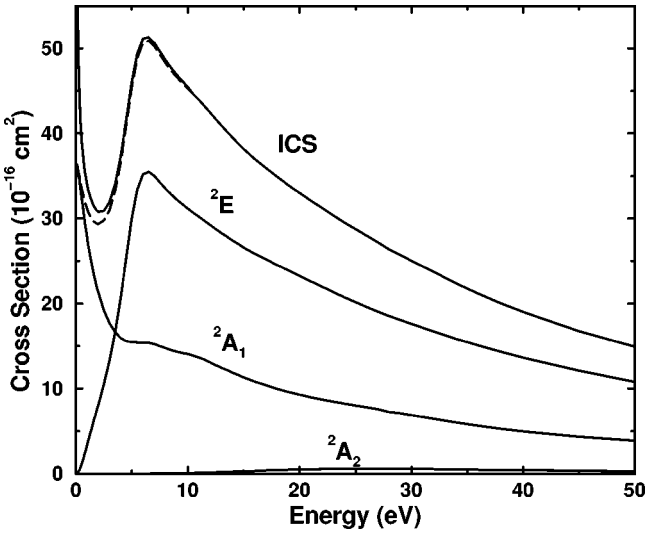

FIG. 1. Integral cross section for elastic scattering of electrons by CH_3SiH_3, along with its C_{3v} symmetry components. Below 10 eV, the integral cross section is shown both with (solid line) and without (dashed line) a correction for long-range scattering.

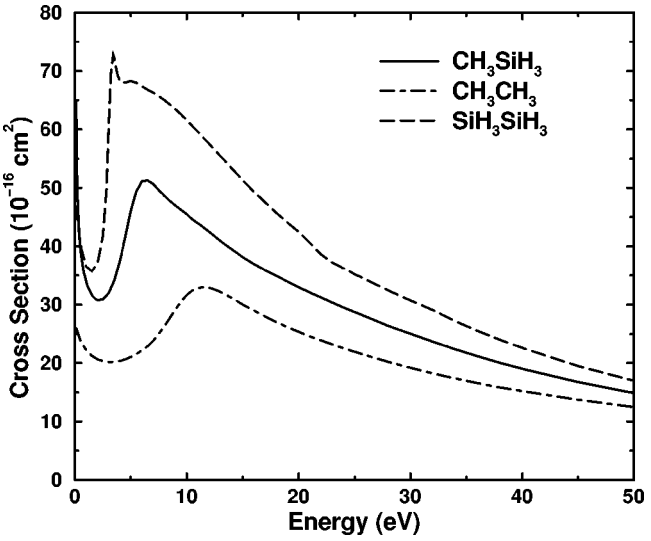

FIG. 2. Comparison of the calculated integral cross sections for elastic scattering of electrons by CH_3SiH_3 with cross sections obtained at the same level of approximation for C_2H_6 and Si_2H_6.

and differed from each other by less than 1% at all energies shown (and by less than 0.5% above 5 eV). For the symmetry components, we show only results without the dipole-Born correction, while for the ICS itself, we show results both with and without the dipole-Born correction below 10 eV. As may be seen, the correction is quite small above ~ 2 eV, while at 2 eV and lower energies, we expect the computed cross section to be qualitatively incorrect due to excessive *s*-wave scattering, a characteristic feature of the static-exchange approximation that produces the low-energy enhancement of $^2A_1$ seen in the figure.

The $^2A_2$ component, having contributions only from partial waves with $m_z \geqslant 3$, is both expected and found to be small over the energy range of Fig. 1, although the calculation probably gives somewhat too small a value at the higher energies shown, because only a few functions in our Gaussian basis set (the *p* functions on the hydrogens) can contribute to the $^2A_2$ trial wave function. The main contributions to the ICS come from $^2A_1$ and ^2E. While neither of these shows any sharp resonance features, at least two broad shoulders visible in $^2A_1$, at about 6.5 and 10 eV, as well as a broad peak in ^2E at about 6.5 eV, may be associated with shape resonances. Because low-energy shape resonances are almost always associated with virtual valence orbitals, insight into them can often be gained from a consideration of the number, type, and energies of RHF virtual orbitals computed in a minimal basis set, though the RHF orbital energies typically must be shifted downward by several eV or more to obtain reasonable agreement with resonance positions. In the present case, minimal-basis-set RHF calculations (obtained with GAMESS and its internal STO-6G basis) place the virtual valence orbitals at 12.2 eV ($8a_1$, Si–C σ^*), 12.7 eV ($4e$, Si–H σ^*), 14.2 eV ($9a_1$, Si–H σ^*), 19.3 eV ($5e$, C–H σ^*), and 20.2 eV ($10a_1$, C–H σ^*). The first three of these orbitals correlate fairly well with the cross-section shoulders and peaks noted, if shifts of 4 to 6 eV are applied. Similar shifts applied to the C–H σ^* orbitals lead to an expectation of resonances in both $^2A_1$ and ^2E near 15 eV; that no such features are visible in Fig. 1 suggests that any such resonances must be very weak and/or broad.

In Fig. 2 we compare the elastic ICS of CH_3SiH_3 with the static-exchange cross sections for the closely related molecules ethane (CH_3CH_3) and disilane (SiH_3SiH_3). Over the energy range studied, the CH_3SiH_3 ICS is everywhere larger than the CH_3CH_3 ICS and is smaller than the SiH_3SiH_3 ICS everywhere except the very lowest energies, where dipolar scattering enhances the CH_3SiH_3 cross section. That the scattering cross section should generally increase with increasing target electron count and geometric size (the order of bond lengths being $r_{CC} < r_{SiC} < r_{SiSi}$) is a natural expectation, though one that is more strictly justified for the *total* scattering cross section than for the elastic component alone.

We expect, as mentioned earlier, that the static-exchange resonance positions we have calculated will lie above the actual resonance positions by ~ 1 to a few eV. As a point of reference, measurements on disilane[27] show a pronounced resonance at about 2 eV that we assign to the ^2E shape resonance that our calculation places at about 3.4 eV (see Fig. 2).

In Fig. 3 we compare the momentum transfer cross section (MTCS) for methylsilane with the MTCS for ethane and disilane. Above 30 eV, the magnitude of the MTCS correlates with molecular size, as was the case for the ICS at all energies; however, the MTCS of all three molecules are approximately equal from about 10 to 30 eV, while below 10 eV the differences among the MTCS appear to have more to do with the prominence of the shape resonances than with molecular size (though the Si_2H_6 MTCS is in fact largest, and the C_2H_6 MTCS smallest, in that range). The Si_2H_6 MTCS, in particular, shows a strong peak near 3.4 eV which may be attributed to the ^2E shape resonance at that energy; this peak is also visible in the ICS (Fig. 2) but is there less prominent compared to a $^2A_1$ resonance at about 5.2 eV,

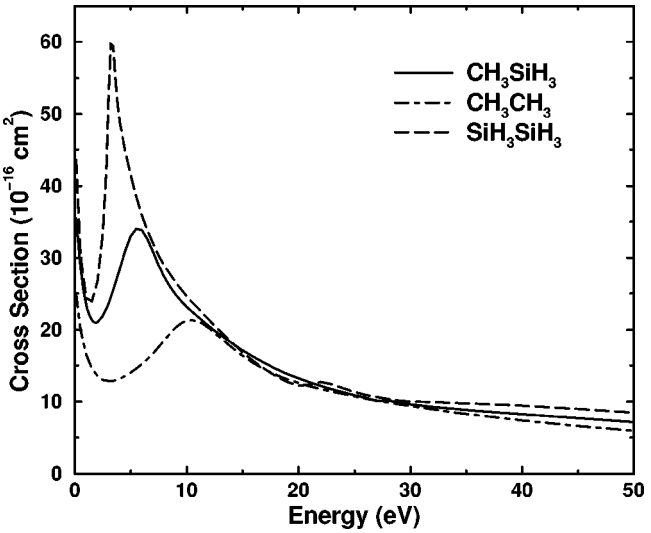

FIG. 3. Comparison of the calculated momentum-transfer cross sections for elastic scattering of electrons by C_2H_6, CH_3SiH_3, and Si_2H_6.

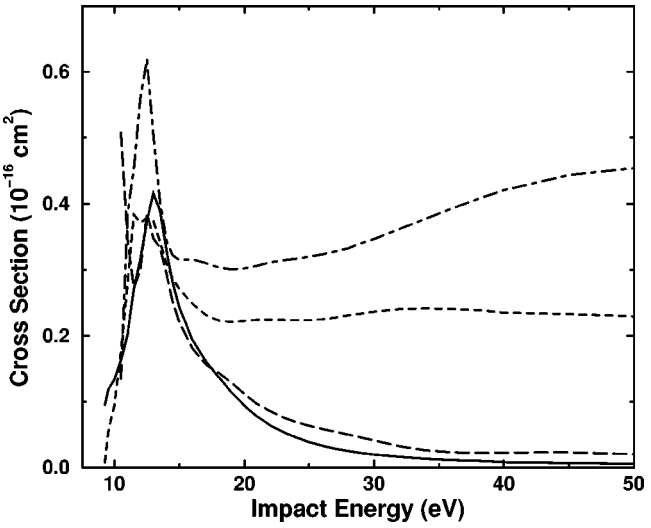

FIG. 5. Computed integral cross sections for electron-impact excitation of the $(7a_1 \rightarrow 8a_1)\ ^3A_1$ (solid line), $(7a_1 \rightarrow 8a_1)\ ^1A_1$ (short dashes), $(7a_1 \rightarrow 9a_1)\ ^3A_1$ (long dashes), and $(7a_1 \rightarrow 9a_1)\ ^1A_1$ (dot-dashed line) transitions in CH_3SiH_3.

indicating that the ^2E resonance has a greater influence on high-angle scattering.

The elastic differential cross sections (DCS) for CH_3SiH_3 are shown at selected energies in Fig. 4. Results for C_2H_6 and Si_2H_6 are again shown for comparison. The effect of the dipole interaction on the CH_3SiH_3 DCS is seen to be insignificant except at angles very near 0°. There is little resemblance among the cross sections of the different molecules. At 5 eV the effect of the ^2E resonance on high-angle scattering by Si_2H_6 is evident, while the C_2H_6 DCS shows structure at 10 eV that may be associated with a broad shape resonance there. At higher energies the cross sections become increasingly forward-peaked and increasingly oscillatory at high angles, with these trends being most pronounced for the largest molecule, Si_2H_6, and least pronounced for C_2H_6.

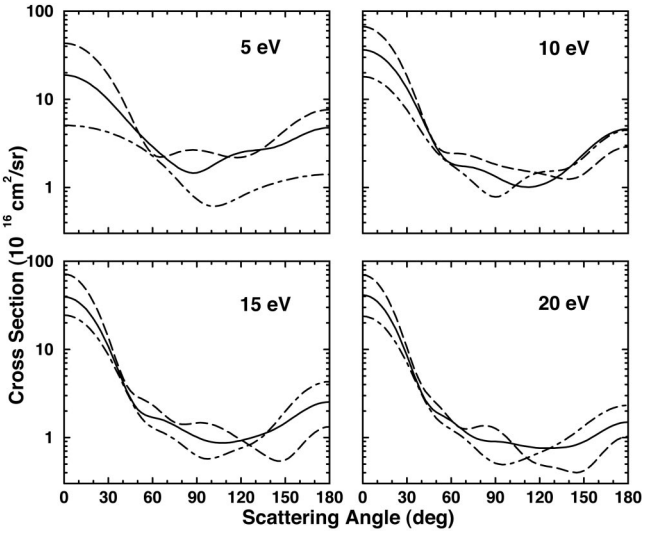

FIG. 4. Differential cross section for elastic electron scattering by CH_3SiH_3 at selected energies, with results for C_2H_6 and Si_2H_6 shown for comparison.

B. Inelastic scattering

Figure 5 shows the integral cross sections for electron-impact excitation of the $(7a_1 \rightarrow 8a_1)\ ^{1,3}A_1$ and $(7a_1 \rightarrow 9a_1)\ ^{1,3}A_1$ states. Each of the cross sections in Fig. 5 displays a peak centered near 12 or 13 eV. Symmetry decomposition (not shown) indicates that in each case both $^2A_1$ and ^2E contribute to the peak in approximately equal amounts except for $(7a_1 \rightarrow 9a_1)\ ^1A_1$, where ^2E accounts for about 2/3 of the cross section, with this "extra" contribution from ^2E roughly accounting for the difference in peak height between $3\ ^1A_1$ and the other three channels. Above 20 eV, the singlet cross sections are increasingly dominated by the long-range scattering accounted for by the dipole-Born correction, while the triplet cross sections fall off rapidly, as expected for spin-changing excitations.

The peaks in the cross sections of Fig. 5 may be due to core-excited shape resonances, which could arise by the same mechanism as the shape resonances in the elastic channel, that is, temporary trapping in empty valence orbitals. Such an origin would make the strong resemblance among the peaks more understandable, as the states concerned all involve excitation from $7a_1$ to an a_1 Rydberg orbital and so might produce very similar short-range potentials.

In Fig. 6 we present the integral cross sections for excitation of the $(3e \rightarrow 8a_1)\ ^{1,3}E$ and $(3e \rightarrow 9a_1)\ ^{1,3}E$ states. As was the case with the $7a_1 \rightarrow 8,9a_1$ excitations, there is an overall resemblance among the cross sections, although in the present case the two singlet cross sections differ greatly in magnitude, and moreover the $(7a_1 \rightarrow 8a_1)\ ^1A_1$ cross section shows only a single maximum at about 12.5 eV, while the other three channels have maxima near 13 eV and near 15 eV. Symmetry decomposition again indicates that both $^2A_1$ and ^2E contribute to the peaks in the cross sections.

Cross sections for the $(7a_1 \rightarrow 4e)\ ^{1,3}E$ excitations are shown in Fig. 7. Comparison with Fig. 5 shows that these cross section are qualitatively similar not only to each other

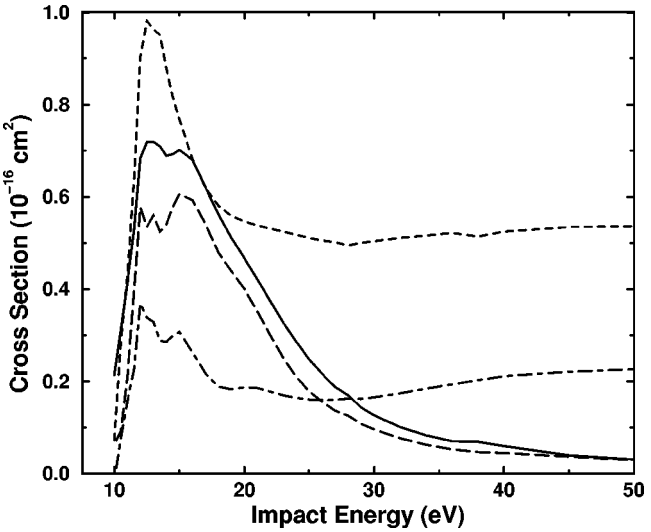

FIG. 6. Computed integral cross sections for electron-impact excitation of the $(3e\rightarrow 8a_1)\ ^3E$ (solid line), $(3e\rightarrow 8a_1)\ ^1E$ (short dashes), $(3e\rightarrow 9a_1)\ ^3E$ (long dashes), and $(3e\rightarrow 9a_1)\ ^1E$ (dot-dashed line) transitions in CH_3SiH_3.

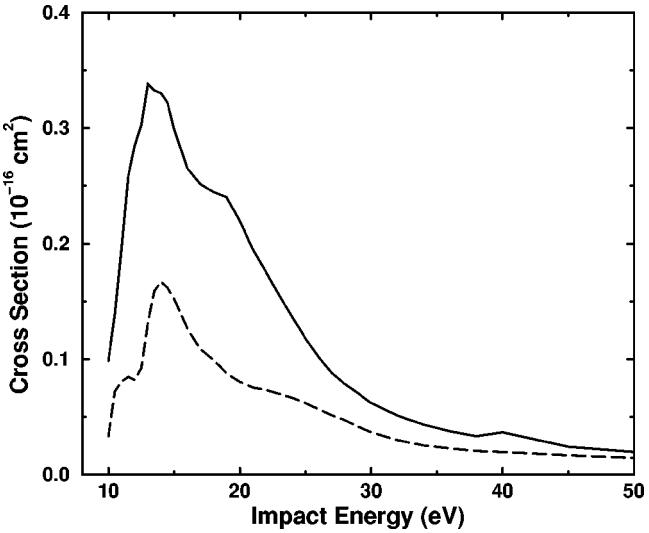

FIG. 8. Computed integral cross sections for electron-impact excitation of the $(3e\rightarrow 4e)\ ^3A_2$ (solid line) and $(3e\rightarrow 4e)\ ^1A_2$ (dashes) transitions in CH_3SiH_3.

but to those for the $7a_1\rightarrow na_1$ excitations, the principal difference, aside from magnitude, being that in the present case the cross section maximum is near 15 rather than 13 eV. Although we have omitted the dipole-Born correction to the singlet cross section in the present case, one can nonetheless observe that the singlet cross section falls off more slowly with energy than does the triplet cross section; inclusion of the dipole correction would somewhat enhance this difference.

The $(3e\rightarrow 4e)\ ^{1,3}A_2$ cross sections are shown in Fig. 8. As described in Sec. II, these are the only physically meaningful excitation cross sections obtained from the $(3e\rightarrow 4e)$ 9-channel calculation. The $^1A_2$ cross section is the smallest, and the $^3A_2$ cross section among the smallest, of the CH_3SiH_3 excitation cross sections we have computed.

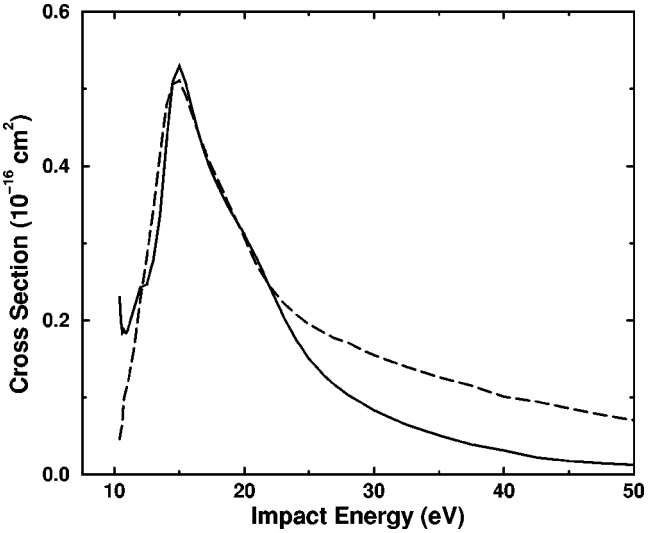

FIG. 7. Computed integral cross sections for electron-impact excitation of the $(7a_1\rightarrow 4e)\ ^3E$ (solid line) and $(7a_1\rightarrow 4e)\ ^1E$ (dashes) transitions in CH_3SiH_3.

Small magnitudes are indeed expected for $A_1\rightarrow A_2$ transitions, which are symmetry-disfavored:[28,29] The excitation amplitude must vanish whenever the scattering plane coincides with one of the three σ_v symmetry planes of CH_3SiH_3 and by continuity must also be small at nearby collision geometries. Moreover, the pattern seen in Fig. 8—the triplet and singlet cross sections being quite similar in form but dissimilar in magnitude, with the singlet cross section significantly smaller—has also been found in calculations for symmetry-disfavored $A_1\rightarrow A_2$ or $\Sigma^+\rightarrow\Sigma^-$ transitions in H_2CO,[28,29] CO,[30,31] N_2,[32] CO_2,[33] and c-C_4F_8.[34] Such a pattern was also seen experimentally in recent studies of N_2, although it is absent or less clear in earlier measurements.[35]

Sources of error affecting our excitation calculations include the use of the single-particle IVO approximation to describe the excited states. As we have mentioned, of the six states nominally arising from the $3e\rightarrow 4e$ excitation, only the $^{1,3}A_2$ states appear to correlate well with physical states of CH_3SiH_3. Neglect of multiconfigurational character may also affect other of our excitation calculations, though probably to a much lesser extent, since most of the other excited states are well described by a one-hole, one-particle picture. However, the SECI calculation indicates that the $3\ ^3A_1$ state, which we have treated as arising solely from $7a_1\rightarrow 9a_1$, in fact contains a strong admixture of $3e\rightarrow ne$. Also, our use of a common IVO orbital to represent both singlet and triplet states having the same nominal configuration may not always be a good approximation. Other sources of error that should be mentioned include numerical sensitivity that, especially near threshold, can introduce unphysical sharp features and some uncertainty in the excitation cross section magnitude; neglect of core relaxation, which may cause core-excited resonances to appear too high in energy, possibly even causing Feshbach resonances to appear as core-excited resonances; use of the IVO thresholds, which are higher than the true vertical thresholds; and use of the IVO transition dipole moments, which may contain significant er-

rors, to compute the dipole-scattering corrections. Finally it should be mentioned that we have not explored the effect, which may be large, of changing the channel-coupling scheme, either among open channels or by including closed-channel (polarization) effects.

With these limitations in mind, our most reliable excitation results are probably those for the $2\,^{1,3}A_1$, $1{,}2\,^{1,3}E$, $1\,^{1,3}A_2$, and $3\,^1A_1$ states, a set that includes the lowest four states in each of the singlet and triplet manifolds. Because electron energy distributions in materials-processing plasmas are typically peaked at 1 to a few eV, these low-lying states will be especially important to electron-driven dissociation. As we have mentioned earlier, the $2\,^{1,3}A_1$ states appear to dissociate without a barrier to methyl and silyl radicals, while calculations indicate that the $1\,^{1,3}E$ states dissociate to CH_3SiH and H_2. Because the next few excited states also involve removal of an electron from either the $7a_1$ Si–C bonding orbital or the $3e$ Si–H bonding orbital and may moreover cross onto these lower surfaces, they are likely to dissociate similarly. When shifted to appropriate thresholds, our cross sections may therefore form a starting point for modeling electron-impact dissociation of CH_3SiH_3.

IV. SUMMARY

We have reported cross sections for elastic and electronically inelastic collisions of low-energy electrons with methylsilane, CH_3SiH_3. The elastic cross sections are intermediate in character between those of the related molecules C_2H_6 and Si_2H_6. The inelastic cross sections studied, which involve transitions from the highest two valence orbitals into predominantly Rydberg orbitals, show strong similarities among themselves, and they are likely to promote two primary dissociation processes.

ACKNOWLEDGMENTS

This work was supported by the U.S. Department of Energy, Office of Basic Energy Sciences, and by the U.S. National Science Foundation under the U.S.–Brazil Cooperative Research program. M.H.F.B. acknowledges support from Brazilian agency Conselho Nacional de Desenvolvimento Científico Tecnológico (CNPq), from the Paraná state agency Fundação Araucária, and from FUNPAR. We are grateful to Intel Corporation for an equipment grant used to construct the computer cluster where most of these calculations were run. Calculations were also performed using facilities of CENAPAD-SP, of the Center for Advanced Computing Research (CACR) at the California Institute of Technology, and of the JPL/Caltech Supercomputer Project. The authors are grateful for assistance of CACR staff, especially Sharon Brunett and Heidi Lorenz-Wirzba.

[1] See, for example, C. W. Lin and J. C. Sturm, J. Appl. Phys. **82**, 4558 (1997); M. S. Lee and S. F. Bent, J. Phys. Chem. B **101**, 9195 (1997); J. L. Hoyt, T. O. Mitchell, K. Rim, D. V. Singh, and J. F. Gibbons, Thin Solid Films **321**, 41 (1998); A. C. Mocuta and D. W. Greve, J. Appl. Phys. **85**, 1240 (1999).

[2] See, for example, R. L. Kostelak, T. W. Weidman, S. Vaidya, O. Joubert, S. C. Palmateer, and M. Hibbs, J. Vac. Sci. Technol. B **13**, 2994 (1995); C. Monget and O. Joubert, *ibid.* **18**, 785 (2000); O. Joubert, D. Fuard, C. Monget, and T. Weidman, *ibid.* **18**, 793 (2000); C. Monget, O. Joubert, and R. L. Inglebert, *ibid.* **18**, 2534 (2000).

[3] See, for example, I. Golecki, F. Reidinger, and J. Marti, Appl. Phys. Lett. **60**, 1703 (1992); A. D. Johnson, J. Perrin, J. A. Mucha, and D. E. Ibbotson, J. Phys. Chem. **97**, 12937 (1993); Y. Ohshita, J. Phys. Chem. **147**, 111 (1995).

[4] See, for example, D. G. Shamiryan, M. R. Baklanov, S. Vanhaelemeersch, and K. Maex, Electrochem. Solid-State Lett. **4**, F3 (2001); Z.-C. Wu, Z.-W. Shiung, C.-C. Chiang, W.-H. Wu, M.-C. Chen, S.-M. Jeng, W. Chang, P.-F. Chou, S.-M. Jang, C.-H. Yu, and M.-S. Liang, J. Electrochem. Soc. **148**, F127 (2001).

[5] C. Winstead and V. McKoy, Adv. At., Mol., Opt. Phys. **43**, 111 (2000).

[6] See, for example, A. Komornicki, J. Am. Chem. Soc. **106**, 3114 (1984); S. Mathews, J. L. Duncan, D. C. McKean, and B. A. Smart, J. Mol. Struct. **413**, 553 (1997); J. Kaski, P. Lantto, T. T. Rantala, J. Schroderus, J. Vaara, and J. Jokisaari, J. Phys. Chem. A **103**, 9669 (1999).

[7] See, for example, D. R. Gano, M. S. Gordon, and J. A. Boatz, J. Am. Chem. Soc. **113**, 6711 (1991); S. Sakai and M. Nakamura, J. Phys. Chem. **97**, 4960 (1993); K. A. Nguyen, M. S. Gordon, and K. Raghavachari, J. Phys. Chem. **98**, 6704 (1994).

[8] M. S. Gordon, J. Chem. Phys. **76**, 3049 (1982).

[9] Y. Harada, J. N. Murrell, and H. H. Sheena, Chem. Phys. Lett. **1**, 595 (1968).

[10] A. G. Alexander, O. P. Strausz, R. Pottier, and G. P. Semeluk, Chem. Phys. Lett. **13**, 608 (1972).

[11] R. Roberge, C. Sandorfy, J. I. Matthews, and O. P. Strausz, J. Chem. Phys. **69**, 5105 (1978).

[12] C. A. S. Maia and M. H. F. Bettega, Phys. Rev. A **63**, 042710 (2003).

[13] O. P. Strausz, K. Obi, and W. K. Duholke, J. Am. Chem. Soc. **90**, 1359 (1968).

[14] K. Obi, A. Clement, H. E. Gunning, and O. P. Strausz, J. Am. Chem. Soc. **91**, 1622 (1969).

[15] P. A. Longeway and F. W. Lampe, J. Photochem. **14**, 311 (1980).

[16] K. Takatsuka and V. McKoy, Phys. Rev. A **24**, 2473 (1981); **30**, 1734 (1984).

[17] M. A. P. Lima, L. M. Brescansin, A. J. R. da Silva, C. Winstead, and V. McKoy, Phys. Rev. A **41**, 327 (1990).

[18] C. Winstead and V. McKoy, Adv. At., Mol., Opt. Phys. **36**, 183 (1996).

[19] C. Winstead and V. McKoy, Comput. Phys. Commun. **128**, 386 (2000).

[20] M. W. Schmidt, K. K. Baldridge, J. A. Boatz *et al.*, J. Comput. Chem. **14**, 1347 (1993).

[21] *CRC Handbook of Chemisjtry and Physics*, 73rd ed., edited by D. R. Lide (CRC, Boca Raton, FL, 1992).

[22] M. J. Frisch, G. W. Trucks, H. B. Schlegel *et al.*, GAUSSIAN 98, Revision A.5, Gaussian, Inc., Pittsburgh, PA, 1998.

[23] T. N. Rescigno and B. I. Schneider, Phys. Rev. A **45**, 2894 (1992), and references therein.

[24] A. Almenningen and O. Bastiansen, Acta Chem. Scand. **9**, 815 (1955).

[25] B. Beagley, A. R. Conrad, J. M. Freeman, J. J. Monaghan, and B. G. Norton, J. Mol. Struct. **11**, 371 (1972).

[26] W. J. Hunt and W. A. Goddard, Chem. Phys. Lett. **3**, 414 (1969).

[27] M. A. Dillon, L. Boesten, H. Tanaka, M. Kimura, and H. Sato, J. Phys. B **27**, 1209 (1994).

[28] T. N. Rescigno, B. H. Lengsfield III, and C. W. McCurdy, Phys. Rev. A **41**, 2462 (1990).

[29] Q. Sun, C. Winstead, V. McKoy, J. S. E. Germano, and M. A. P. Lima, Phys. Rev. A **46**, 2462 (1992).

[30] Q. Sun, C. Winstead, and V. McKoy, Phys. Rev. A **46**, 6987 (1992).

[31] L. A. Morgan and J. Tennyson, J. Phys. B **26**, 2429 (1993).

[32] H. P. Pritchard, Ph.D. thesis, California Institute of Technology, Pasadena, California, 1994.

[33] C.-H. Lee, C. Winstead, and V. McKoy, J. Chem. Phys. **111**, 5056 (1999).

[34] C. Winstead and V. McKoy, J. Chem. Phys. **114**, 7407 (2001).

[35] L. Campbell, M. J. Brunger, A. M. Nolan, L. J. Kelly, A. B. Wedding, J. Harrison, P. J. O. Teubner, D. C. Cartwright, and B. McLaughlin, J. Phys. B **34**, 1185 (2001), and references therein.